Available online at www.sciencedirect.com

ScienceDirect

Physics Procedia 63 (2015) 11 – 20

Physics Procedia

43rd Annual Symposium of the Ultrasonic Industry Association, UIA Symposium 2014

Optimizing piezoelectric stack preload bolts in ultrasonic transducers

D. A. DeAngelis, G. W. Schulze and K. S. Wong

Mechanical Engineering, Ultrasonics Group, Kulicke & Soffa Industries, 1005 Virginia Drive, Fort Washington, PA 19034, USA

Abstract

The selection of the preload bolt is often an afterthought in the design of Langevin type "sandwich" transducers, but quite often it is the root cause of failure for power ultrasonic applications. The main role of the preload bolt is to provide a "prestress" in the piezo stack to prevent interface "gapping" or tension in glued joints which can result in delamination. But as an integral part of a highly tuned dynamic system, the resulting parasitic resonances in these preload bolts, such as bending or longitudinal modes, are often difficult to predict and control. This research investigates many aspects of preload bolt design for achieving optimal transducer performance, including basic size and strength determination based on drive amplitude, as well as ensuring adequate thread engagement to the mating horn. Other aspects such as rule-of-thumb configuration and length guidelines to reduce parasitic resonances are also investigated. Optimizing the uniformity of stress in the piezoceramics is also considered, which is affected by end mass length, counterbores and proximity to threading. The selection of the bolt material based on stiffness is also investigated as related to electromechanical coupling. The investigation focuses solely on Langevin type transducers used for semiconductor wire bonding, and which are comprised of the common Navy Types I and III (PZT4 and PZT8) piezoelectric materials. Several metrics are investigated such as impedance, displacement gain, and electromechanical coupling factor. The experimental and theoretical research methods include Bode plots, scanning laser vibrometry and finite element analysis.

© 2015 The Authors. Published by Elsevier B.V. This is an open access article under the CC BY-NC-ND license
(http://creativecommons.org/licenses/by-nc-nd/4.0/).
Peer-review under responsibility of the Ultrasonic Industry Association

Keywords: Ultrasonic transducer; Preload bolts; Prestress; Piezoceramic; PZT8; Power ultrasonics; Langevin; Wire bonding

---

1. Introduction

The selection of the preload bolt is often an afterthought in the design of Langevin type "sandwich" transducers. Even within transducer design companies such as Kulicke & Soffa Industries, there is no consistent methodology for design or configuration of preload bolts. Quite often the preload bolt is the root cause of failure for power ultrasonic transducers (e.g., yield/breakage, preload loss, parasitic mode). The main role of the preload bolt is to provide a "prestress" in the piezo stack to prevent interface "gapping" or tension in glue joints (delamination). Preload bolts

1875-3892 © 2015 The Authors. Published by Elsevier B.V. This is an open access article under the CC BY-NC-ND license
(http://creativecommons.org/licenses/by-nc-nd/4.0/).
Peer-review under responsibility of the Ultrasonic Industry Association
doi:10.1016/j.phpro.2015.03.003

are an integral part of the highly tuned dynamic system. Resulting parasitic resonances in preload bolts such as bending or longitudinal modes are often difficult to predict and control. Some rule-of-thumb design and configuration guidelines for preload bolts are needed.

2. Specific transducer application

Kulicke & Soffa Industries is the leading manufacturer of semiconductor wire bonding equipment. This "back-end" type of equipment provides ultrasonically welded interconnect wires or ribbons between the wafer level semiconductor circuitry and the mounting package as shown in Fig. 1. The ultrasonic transducer delivers energy to a wedge or capillary tool for welding wire or ribbons (typically aluminum or copper) (DeAngelis et al., 2006, 2011, 2012). As is easily seen in Fig. 1, many different preload bolt configurations have been used for the various transducer designs.

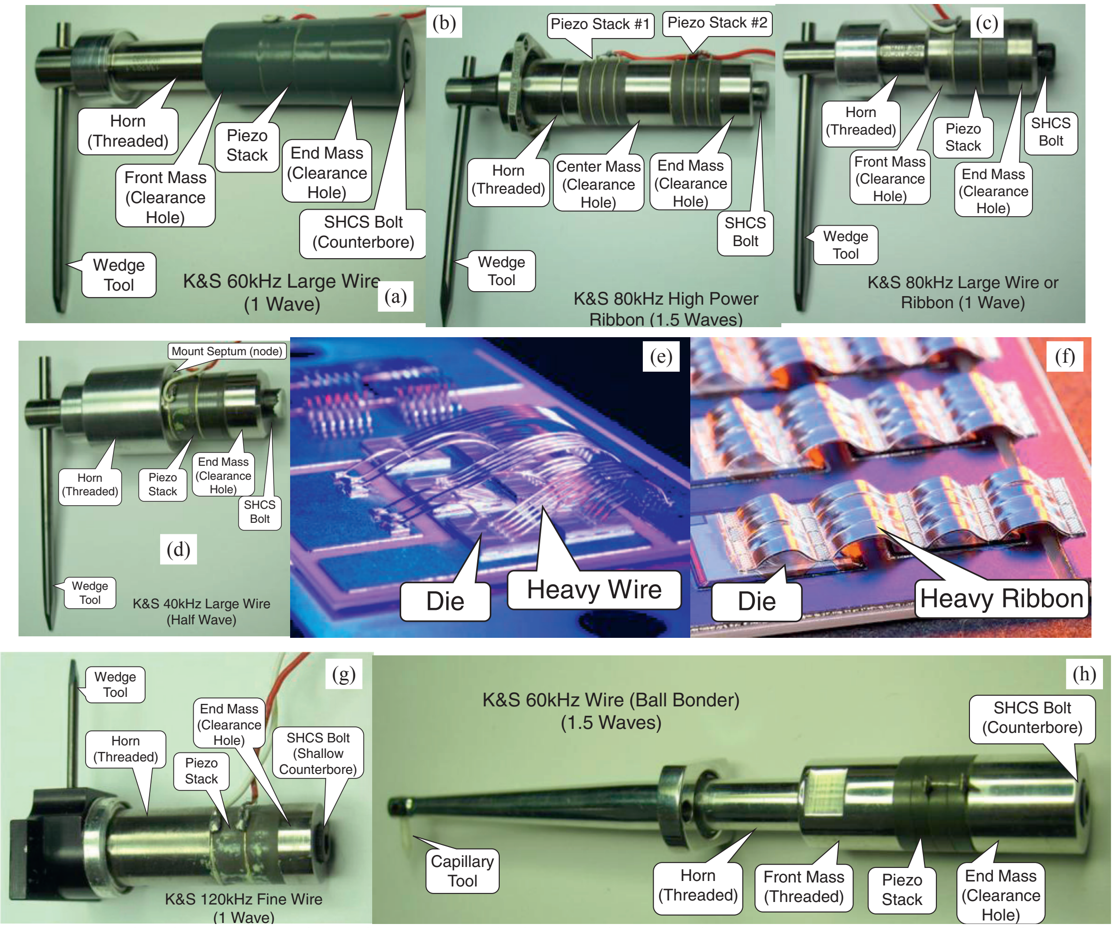

Fig. 1. (a) K&S 60kHz large wire transducer, (b) K&S 80kHz high power ribbon transducer, (c) K&S 80kHz large wire or ribbon, (d) K&S 40kHz large wire, (e) Heavy wire device, (f) Heavy ribbon device, (g) K&S 120kHz fine wire, (h) K&S 60kHz wire (ball bonder).

3. Common preload bolt configurations

Figs. 2 through 6 show the pros and cons of common preload bolt configurations (Wilson, 1991, Sherman et al., 2007, Stansfield, 1991). From a dynamic standpoint, the preload screw should be fairly well behaved at the operating mode of the transducer, such that there are no parasitic resonances in the preload screw near the operating mode. Also, absent of parasitic modes the symmetry of the free length of the preload screw relative to the piezo stack will determine if the operating node in the stack and screw are co-located: this can be important for aging considerations and for glue filling due to relative motions; it should also be noted that the location of parasitic screw modes can be inconsistent with glued piezo stack designs when considering dry versus glued designs. From a static standpoint, the preload screw configuration should provide a uniform stress distribution over the piezoceramics to utilize this active material most efficiently; both the electromechanical coupling and maximum drive level are degraded with non-uniform stress (Woollett, 1957).

4. Failure modes in preload screws

Fig. 7 shows the finite element model for analyzing failure modes in the preload screw for the 80kHz large wire transducer shown in Fig. 1(c). Fig. 8 shows actual screw failures with an assessment overview including effects from glue bridging (can move parasitic screw mode frequencies), and static finite element modeling to illustrate the degree of non-uniform stress in the piezo stack due to preload bolt loading. As shown in Fig 7(b), the screw resonance mode here may be described as "slinky-like" (i.e., longitudinal mode), since the screw mode has "one end" out of phase with the natural driver motion. This situation has the potential to exert very high loads at the preload screw threads, as shown by the breakage in Fig. 8. It should be noted that alternate axisymmetric FEA models would have predicted this slinky mode, but will have missed all the bending modes in screw (common mistake).

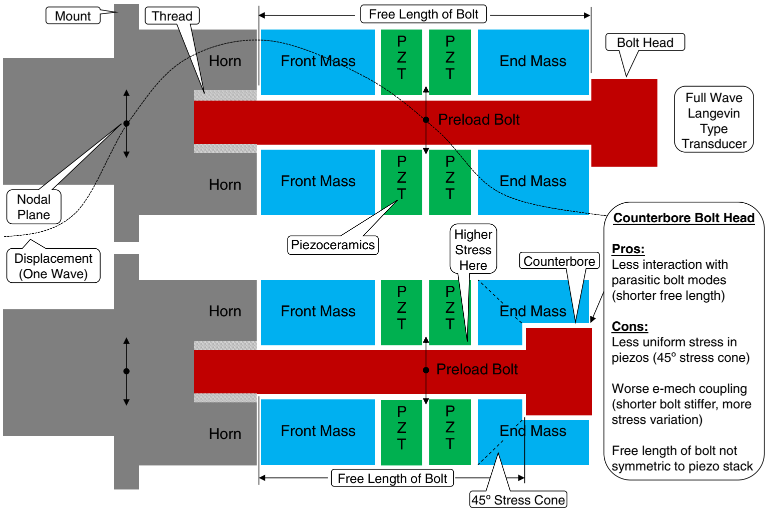

Counterbore Bolt Head

Pros:
Less interaction with parasitic bolt modes (shorter free length)

Cons:
Less uniform stress in piezos (45° stress cone)

Worse e-mech coupling (shorter bolt stiffer, more stress variation)

Free length of bolt not symmetric to piezo stack

Fig. 2 Pros and cons of a counterbore bolt head configuration for preload screw.

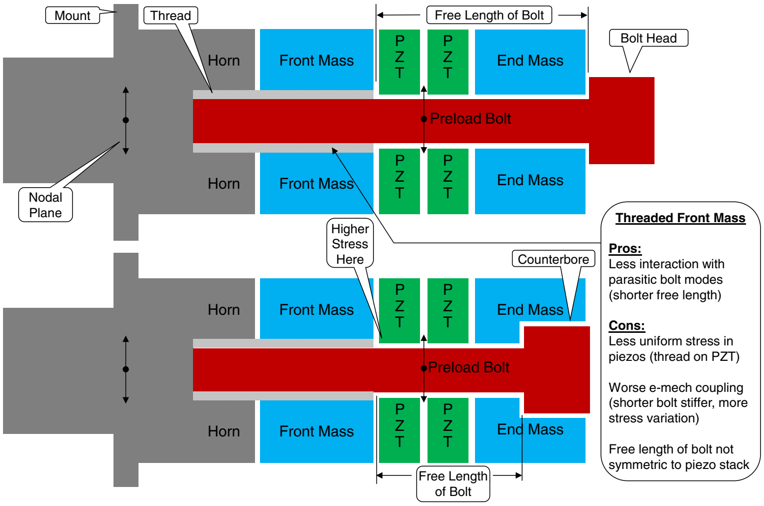

Threaded Front Mass

Pros:
Less interaction with parasitic bolt modes (shorter free length)

Cons:
Less uniform stress in piezos (thread on PZT)

Worse e-mech coupling (shorter bolt stiffer, more stress variation)

Free length of bolt not symmetric to piezo stack

Fig. 3 Pros and cons of a threaded front mass configuration for preload screw.

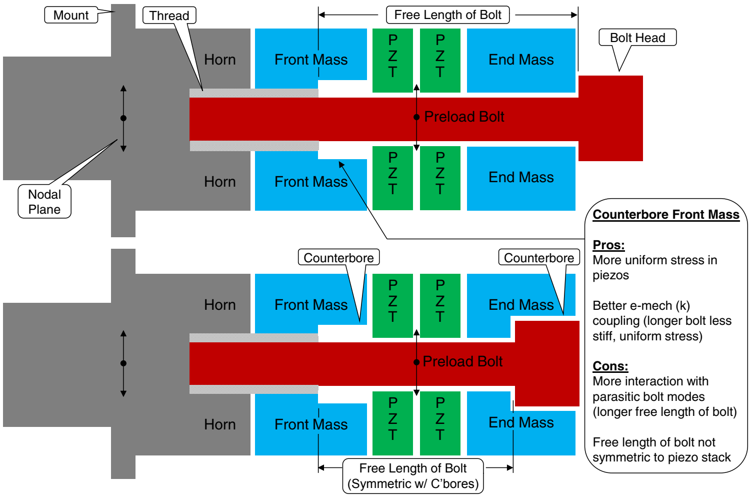

Counterbore Front Mass

Pros:
More uniform stress in piezos

Better e-mech (k) coupling (longer bolt less stiff, uniform stress)

Cons:
More interaction with parasitic bolt modes (longer free length of bolt)

Free length of bolt not symmetric to piezo stack

Fig. 4 Pros and cons of a counterbore front mass configuration for preload screw.

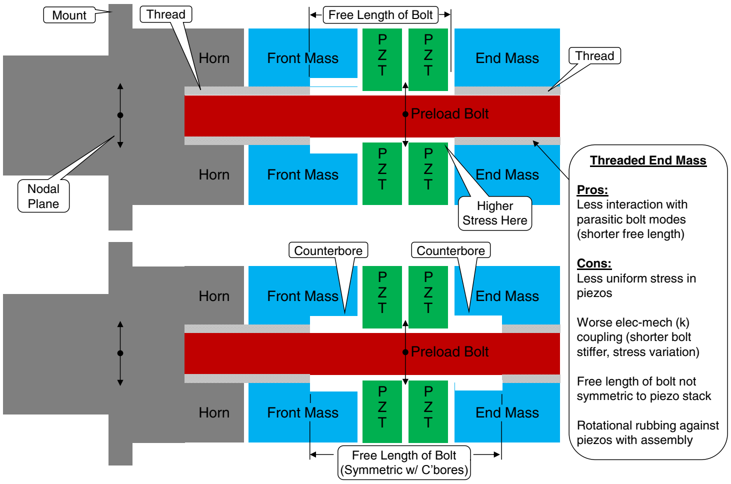

Threaded End Mass

Pros:
Less interaction with parasitic bolt modes (shorter free length)

Cons:
Less uniform stress in piezos

Worse elec-mech (k) coupling (shorter bolt stiffer, stress variation)

Free length of bolt not symmetric to piezo stack

Rotational rubbing against piezos with assembly

Fig. 5 Pros and cons of a threaded end mass configuration for preload screw.

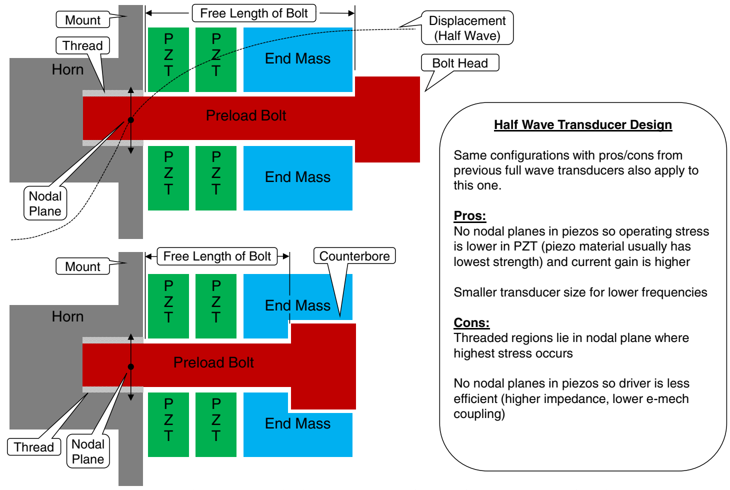

Half Wave Transducer Design

Same configurations with pros/cons from previous full wave transducers also apply to this one.

Pros:
No nodal planes in piezos so operating stress is lower in PZT (piezo material usually has lowest strength) and current gain is higher

Smaller transducer size for lower frequencies

Cons:
Threaded regions lie in nodal plane where highest stress occurs

No nodal planes in piezos so driver is less efficient (higher impedance, lower e-mech coupling)

Fig. 6 Pros and cons of a half wave transducer design for preload screw.

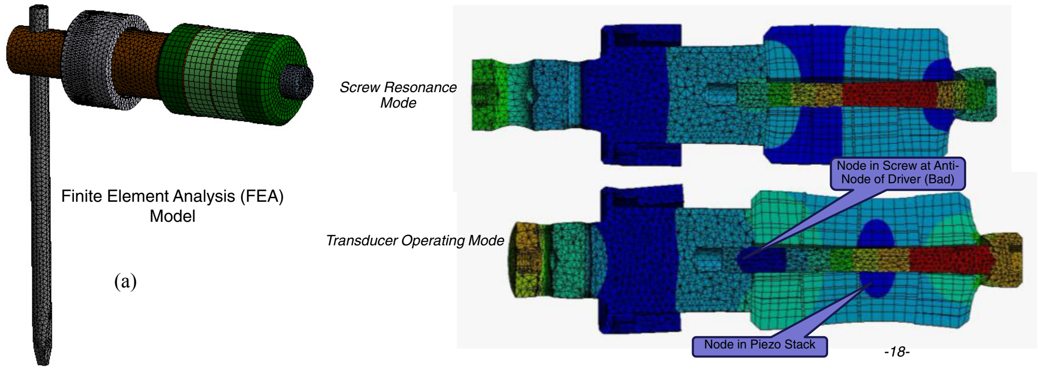

Fig. 7 (a) Finite element model of K&S 80kHz large wire transducer, (b) Preload screw resonance analys sults.

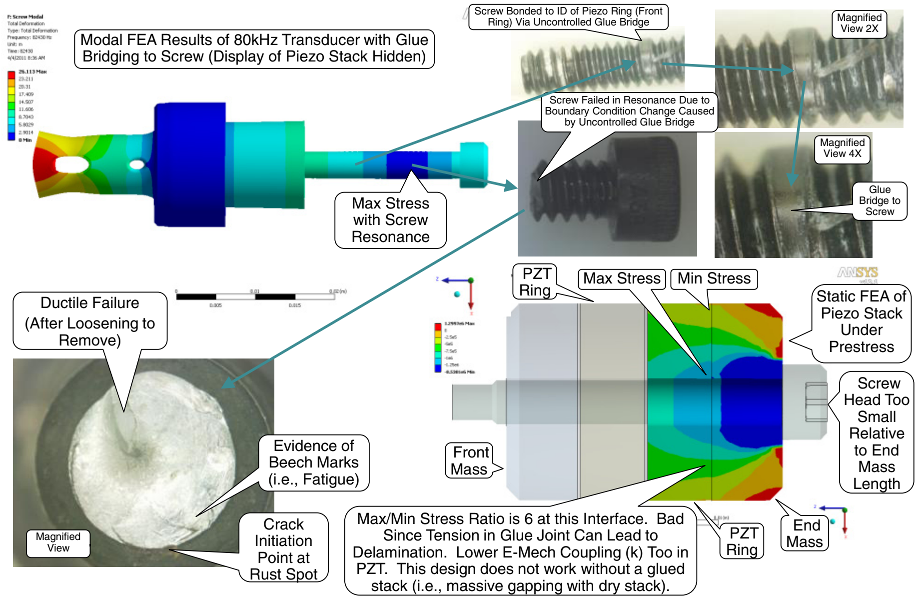

Max/Min Stress Ratio is 6 at this Interface. Bad Since Tension in Glue Joint Can Lead to Delamination. Lower E-Mech Coupling (k) Too in PZT. This design does not work without a glued stack (i.e., massive gapping with dry stack).

Fig. 8 Preload screw resonance analysis with description of actual failure modes.

5. Selection of preload bolt material and sizing of preload bolts

Always use the yield stress, not the tensile strength, when sizing bolts since loss of preload occurs during yielding prior to the bolt breaking. When optimizing for bolt strength, higher strength materials allow the smallest diameter screw, which maximizes volume of the piezo material for a given stack diameter (lower impedance, higher e-mech coupling). Higher strength materials allow for less thread engagement, which minimizes frictional losses (threads can be lossy with higher impedance). When optimizing for transducer electromechanical coupling factor (k), it should be noted that the coupling is proportional to the transducer "phase window" difference of the antiresonance f_a and resonance f_r from the Bode plot (i.e. $k \propto (f_a\text{-}f_r)/f_r$) (DeAngelis et al., 2010, Uchino et al., 2003, Woollett, 1957). The phase window or coupling k is maximized when the bolt stiffness is minimized relative to piezo stack (i.e., least amount of stack energy absorbed by preload screw) (Sherman et al., 2007, Stansfield, 1991). For example, if the preload bolt stiffness is the same as the stack stiffness, then k will be reduced by at least 50% from the max possible k_{33} for the piezo material. The best bolt material is the one with the highest yield strength σ_y and the lowest stiffness or elastic modulus E, i.e., maximize the ratio σ_y /E. The highest yield stress material allows the use of the smallest diameter screw (less stiff). The lowest modulus results in the lowest stiffness for a given diameter. For example, beryllium copper (BeCu, C17300) screws are better than alloy steel screws for maximizing k (i.e., 160/18.5 = 9 versus 170/30 = 6). The coupling k is maximized when the stress in piezo stack is most uniform. Custom screws can be advantageous with necking down in unthreaded areas (reduces stiffness) and flared heads for more uniform stress in piezos; especially with end masses that have poor length/diameter (i.e. L/D) ratios in an attempt to maximize piezo volume. The wave speed (c=sqrt(E/ρ)) is also a consideration for screw design (phasing, node placement, etc.); steel, Ti and Al are about the same, whereas BeCu is 20% less. The uniformity of piezo stress is very important when sizing preload bolts. Nonunifom piezo prestress ultimately results in two simultaneous problems: some volume of the piezo material is insufficiently loaded (i.e. outer diameter of stack) resulting in either tension/delamination in glue joints (for glued stacks) or dynamic gapping at interfaces for dry stacks, and some volume of the piezo material will be overloaded (i.e. inner diameter of stack) resulting in severe depoling (i.e. little or no output). For example, with near uniform prestress in piezo stack (i.e., max/min stress ratio ≈ 1.0) PZT8 materials can withstand 90 MPa of prestress (DeAngelis et al., 2009). However, with max/min stress ratios in the 1.5-3 range, the prestress for PZT8 materials should be reduced to the 30-60 MPa range. For sizing common alloy steel bolts under static prestress, the catalog recommended seating stress of 120 ksi (e.g. Unbrako) is a good guideline. This allows sufficient margin for torqueing and dynamic loading up to 170 ksi yield. The dynamic loading in the bolt is typically less than 10% of prestress levels without resonances. Prestress of 150 ksi can be used for more aggressive designs with a compression load fixture. Figs. 9 and 10 provide guidelines for determining proper thread engagement based on common materials for bolt and internal threads (Walsh, 1990).

Goal: To ensure the length of thread engagement is sufficient to carry the full load necessary to yield the screw without the internal or external threads stripping*

- Tensile Stressed Area of Screw: $A_{ts} = \frac{\pi}{4}\left(D - \frac{0.9743}{n}\right)^2$
- Shear Area of External Thread per Unit Length: $A_{se} = \pi n D_m \left(\frac{1}{2n} + \frac{P_d - D_m}{\sqrt{3}}\right)$
- Shear Area of Internal Thread per Unit Length: $A_{si} = \pi n D_M \left(\frac{1}{2n} + \frac{D_M - D_p}{\sqrt{3}}\right)$

Common design mistake is to use tensile strength for determining minimum thread engagement.

Failure for a transducer must be defined by the yielding of threads where preload is lost.

where D = major diameter, n = number of threads per inch, D_m = max minor diameter of internal thread, D_p = max pitch diameter of internal thread, P_d = min pitch diameter of external thread, and D_M = min major diameter of external thread

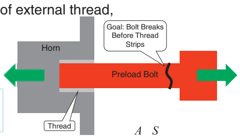

- To Determine Minimum Thread Engagement Length, E_L:
  - A. For same materials for both internal and external threads use: $E_L = \frac{2A_{ts}}{A_{se}}$
  - B. For different materials for internal and external threads, first determine Relative Strength (R), $R = \frac{A_{se} S_e}{A_{si} S_i}$

where S_e = yield strength of external thread material, S_i = yield strength of internal thread material

if $R \leq 1$, use the same equation as A: $E_L = \frac{2A_{ts}}{A_{se}}$

if $R > 1$, use: $E_L = \frac{2A_{ts}}{A_{se}} R = \frac{2A_{ts} S_e}{A_{si} S_i}$

$$\boxed{\sigma_{seating\,(bolt)} = \frac{\sigma_{piezos} A_{piezos}}{A_{stressed\,(bolt)}} = 120\ ksi}$$

*Ref. Walsh or FED-STD-H28/2B

Fig. 9 Preload bolt thread engagement analysis.

❖For example,
with S_e = 170 ksi yield tensile strength for alloy steel screw (class 3A), and S_i = 30 ksi yield tensile strength for annealed 316 stainless steel horn (class 2B), the thread engagement of 8 common UNC screws are:

	D	n	A_{se}	A_{si}	R	A_{ts}	E_L	$E_L(D)$
#2	0.086	56	0.109	0.168	3.683	0.004	0.250	2.9
#4	0.112	40	0.147	0.228	3.659	0.006	0.299	2.7
#6	0.138	32	0.190	0.289	3.724	0.009	0.357	2.6
#8	0.164	32	0.239	0.344	3.924	0.014	0.461	2.8
#10	0.19	24	0.275	0.411	3.788	0.018	0.483	2.5
1/4"	0.25	20	0.383	0.552	3.932	0.032	0.653	2.6
5/16"	0.3125	18	0.489	0.696	3.978	0.052	0.853	2.7
3/8"	0.375	16	0.598	0.845	4.013	0.077	1.040	2.8
							Avg	**2.7**

Tensile strength for annealed 316 stainless is 80 ksi, but yield strength is only 30 ksi. Elongation at failure is a whopping 40%, so if tensile strength is used for the thread engagement length the preload will be long gone before the material can work hardened

Plot of Tensile Stress in Bolt vs Minimum Thread Engagement for:
316 Stainless Steel (annealed), 7075-T6 Aluminum Alloy, and Titanium 6-4 (annealed)

(Class 3A Bolt Threaded in Class 2B Horn)

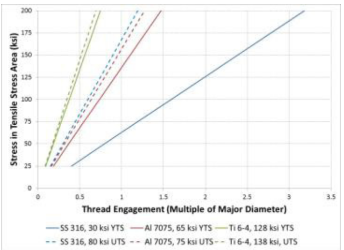

YTS = Yield Stress
UTS = Tensile Strength

Fig. 10 Preload bolt thread engagement example for various materials.

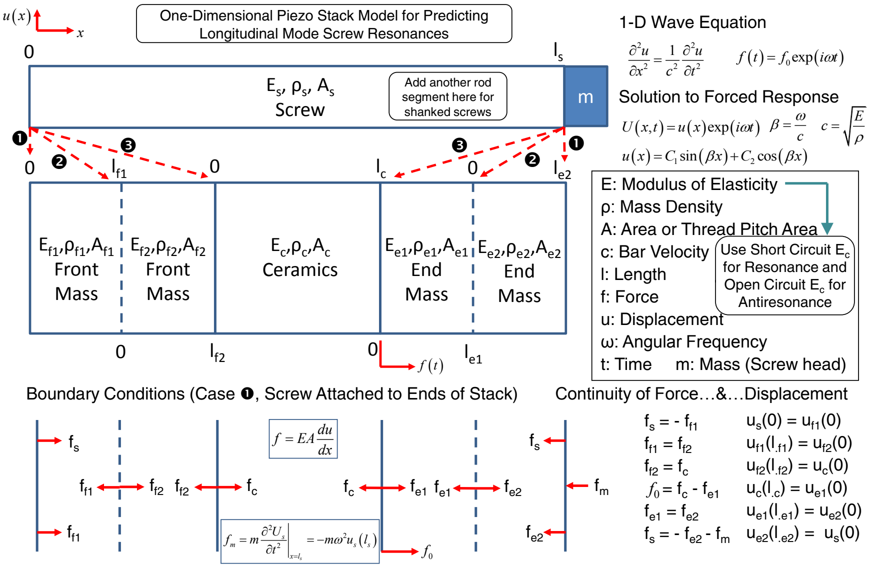

1-D Wave Equation

$$\frac{\partial^2 u}{\partial x^2} = \frac{1}{c^2}\frac{\partial^2 u}{\partial t^2} \qquad f(t) = f_0 \exp(i\omega t)$$

Solution to Forced Response

$$U(x,t) = u(x)\exp(i\omega t) \quad \beta = \frac{\omega}{c} \quad c = \sqrt{\frac{E}{\rho}}$$

$$u(x) = C_1 \sin(\beta x) + C_2 \cos(\beta x)$$

E: Modulus of Elasticity
ρ: Mass Density
A: Area or Thread Pitch Area
c: Bar Velocity
l: Length
f: Force
u: Displacement
ω: Angular Frequency
t: Time m: Mass (Screw head)

Use Short Circuit E_c for Resonance and Open Circuit E_c for Antiresonance

Boundary Conditions (Case ❶, Screw Attached to Ends of Stack)

$$f = EA\frac{du}{dx}$$

$$f_m = m\frac{\partial^2 U_s}{\partial t^2}\bigg|_{x=l_s} = -m\omega^2 u_s(l_s)$$

Continuity of Force…&…Displacement

$f_s = - f_{f1}$	$u_s(0) = u_{f1}(0)$
$f_{f1} = f_{f2}$	$u_{f1}(l_{.f1}) = u_{f2}(0)$
$f_{f2} = f_c$	$u_{f2}(l_{.f2}) = u_c(0)$
$f_0 = f_c - f_{e1}$	$u_c(l_{.c}) = u_{e1}(0)$
$f_{e1} = f_{e2}$	$u_{e1}(l_{.e1}) = u_{e2}(0)$
$f_s = - f_{e2} - f_m$	$u_{e2}(l_{.e2}) = u_s(0)$

Fig. 11 1D modeling for predicting longitudinal mode bolt resonances.

6. Prediction of parasitic bolt resonances

FEA is an excellent method for analyzing existing transducer designs, but it is often not convenient during the initial phases of the transducer design for preload bolts. As shown in Figs 11-17, one dimensional analysis can provide a very accurate, yet fast and simple method for predicting parasitic bolt resonances.

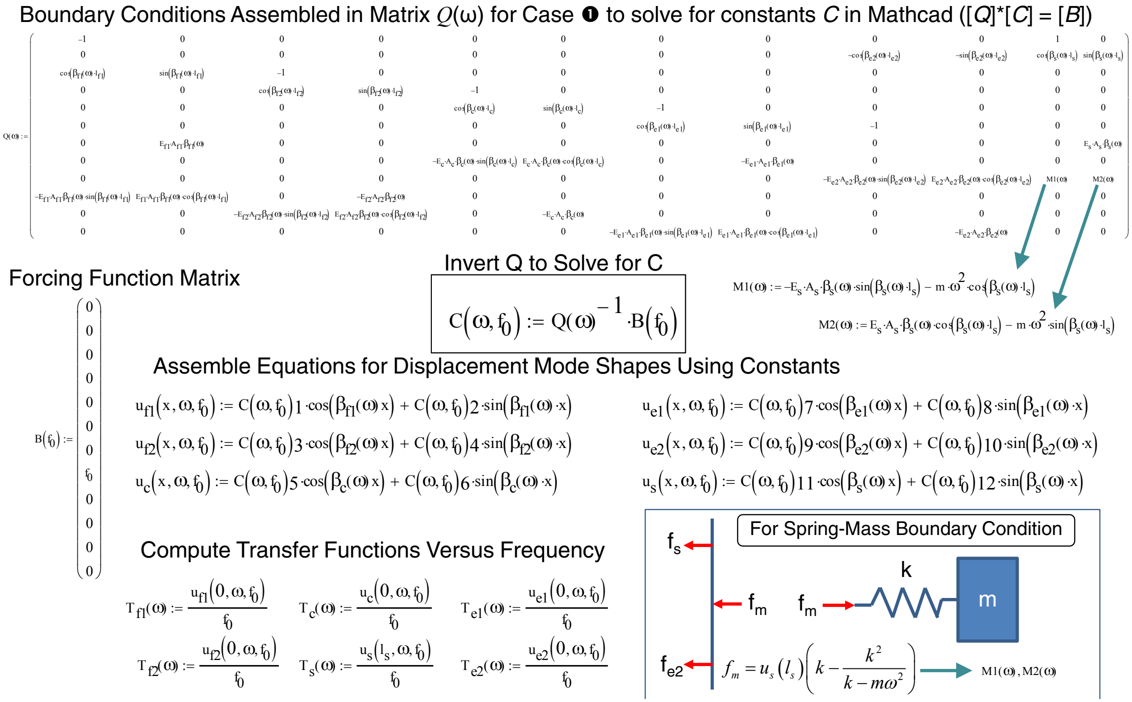

Boundary Conditions Assembled in Matrix $Q(\omega)$ for Case ❶ to solve for constants C in Mathcad ($[Q]*[C] = [B]$)

$$Q(\omega) := \begin{pmatrix} -1 & 0 & 0 & 0 & 0 & 0 & 0 & 0 & 0 & 0 & 1 & 0 \\ 0 & 0 & 0 & 0 & 0 & 0 & 0 & 0 & -\cos(\beta_{e2}(\omega)\cdot l_{e2}) & -\sin(\beta_{e2}(\omega)\cdot l_{e2}) & \cos(\beta_s(\omega)\cdot l_s) & \sin(\beta_s(\omega)\cdot l_s) \\ \cos(\beta_{f1}(\omega)\cdot l_{f1}) & \sin(\beta_{f1}(\omega)\cdot l_{f1}) & -1 & 0 & 0 & 0 & 0 & 0 & 0 & 0 & 0 & 0 \\ 0 & 0 & \cos(\beta_{f2}(\omega)\cdot l_{f2}) & \sin(\beta_{f2}(\omega)\cdot l_{f2}) & -1 & 0 & 0 & 0 & 0 & 0 & 0 & 0 \\ 0 & 0 & 0 & 0 & \cos(\beta_c(\omega)\cdot l_c) & \sin(\beta_c(\omega)\cdot l_c) & -1 & 0 & 0 & 0 & 0 & 0 \\ 0 & 0 & 0 & 0 & 0 & 0 & \cos(\beta_{e1}(\omega)\cdot l_{e1}) & \sin(\beta_{e1}(\omega)\cdot l_{e1}) & -1 & 0 & 0 & 0 \\ 0 & E_{f1}\cdot A_{f1}\cdot\beta_{f1}(\omega) & 0 & 0 & 0 & 0 & 0 & 0 & 0 & 0 & 0 & E_s\cdot A_s\cdot\beta_s(\omega) \\ 0 & 0 & 0 & 0 & -E_c\cdot A_c\cdot\beta_c(\omega)\cdot\sin(\beta_c(\omega)\cdot l_c) & E_c\cdot A_c\cdot\beta_c(\omega)\cdot\cos(\beta_c(\omega)\cdot l_c) & 0 & -E_{e1}\cdot A_{e1}\cdot\beta_{e1}(\omega) & 0 & 0 & 0 & 0 \\ 0 & 0 & 0 & 0 & 0 & 0 & 0 & 0 & -E_{e2}\cdot A_{e2}\cdot\beta_{e2}(\omega)\cdot\sin(\beta_{e2}(\omega)\cdot l_{e2}) & E_{e2}\cdot A_{e2}\cdot\beta_{e2}(\omega)\cdot\cos(\beta_{e2}(\omega)\cdot l_{e2}) & M1(\omega) & M2(\omega) \\ -E_{f1}\cdot A_{f1}\cdot\beta_{f1}(\omega)\cdot\sin(\beta_{f1}(\omega)\cdot l_{f1}) & E_{f1}\cdot A_{f1}\cdot\beta_{f1}(\omega)\cdot\cos(\beta_{f1}(\omega)\cdot l_{f1}) & 0 & -E_{f2}\cdot A_{f2}\cdot\beta_{f2}(\omega) & 0 & 0 & 0 & 0 & 0 & 0 & 0 & 0 \\ 0 & 0 & -E_{f2}\cdot A_{f2}\cdot\beta_{f2}(\omega)\cdot\sin(\beta_{f2}(\omega)\cdot l_{f2}) & E_{f2}\cdot A_{f2}\cdot\beta_{f2}(\omega)\cdot\cos(\beta_{f2}(\omega)\cdot l_{f2}) & 0 & -E_c\cdot A_c\cdot\beta_c(\omega) & 0 & 0 & 0 & 0 & 0 & 0 \\ 0 & 0 & 0 & 0 & 0 & 0 & -E_{e1}\cdot A_{e1}\cdot\beta_{e1}(\omega)\cdot\sin(\beta_{e1}(\omega)\cdot l_{e1}) & E_{e1}\cdot A_{e1}\cdot\beta_{e1}(\omega)\cdot\cos(\beta_{e1}(\omega)\cdot l_{e1}) & 0 & -E_{e2}\cdot A_{e2}\cdot\beta_{e2}(\omega) & 0 & 0 \end{pmatrix}$$

Forcing Function Matrix

$$B(f_0) := \begin{pmatrix} 0 \\ 0 \\ 0 \\ 0 \\ 0 \\ 0 \\ 0 \\ f_0 \\ 0 \\ 0 \\ 0 \\ 0 \end{pmatrix}$$

Invert Q to Solve for C

$$\boxed{C(\omega, f_0) := Q(\omega)^{-1}\cdot B(f_0)}$$

$$M1(\omega) := -E_s\cdot A_s\cdot\beta_s(\omega)\cdot\sin(\beta_s(\omega)\cdot l_s) - m\cdot\omega^2\cdot\cos(\beta_s(\omega)\cdot l_s)$$

$$M2(\omega) := E_s\cdot A_s\cdot\beta_s(\omega)\cdot\cos(\beta_s(\omega)\cdot l_s) - m\cdot\omega^2\cdot\sin(\beta_s(\omega)\cdot l_s)$$

Assemble Equations for Displacement Mode Shapes Using Constants

$$u_{f1}(x,\omega,f_0) := C(\omega,f_0)_1\cdot\cos(\beta_{f1}(\omega)\,x) + C(\omega,f_0)_2\cdot\sin(\beta_{f1}(\omega)\cdot x)$$

$$u_{f2}(x,\omega,f_0) := C(\omega,f_0)_3\cdot\cos(\beta_{f2}(\omega)\,x) + C(\omega,f_0)_4\cdot\sin(\beta_{f2}(\omega)\cdot x)$$

$$u_c(x,\omega,f_0) := C(\omega,f_0)_5\cdot\cos(\beta_c(\omega)\,x) + C(\omega,f_0)_6\cdot\sin(\beta_c(\omega)\cdot x)$$

$$u_{e1}(x,\omega,f_0) := C(\omega,f_0)_7\cdot\cos(\beta_{e1}(\omega)\,x) + C(\omega,f_0)_8\cdot\sin(\beta_{e1}(\omega)\cdot x)$$

$$u_{e2}(x,\omega,f_0) := C(\omega,f_0)_9\cdot\cos(\beta_{e2}(\omega)\,x) + C(\omega,f_0)_{10}\cdot\sin(\beta_{e2}(\omega)\cdot x)$$

$$u_s(x,\omega,f_0) := C(\omega,f_0)_{11}\cdot\cos(\beta_s(\omega)\,x) + C(\omega,f_0)_{12}\cdot\sin(\beta_s(\omega)\cdot x)$$

Compute Transfer Functions Versus Frequency

$$T_{f1}(\omega) := \frac{u_{f1}(0,\omega,f_0)}{f_0} \qquad T_c(\omega) := \frac{u_c(0,\omega,f_0)}{f_0} \qquad T_{e1}(\omega) := \frac{u_{e1}(0,\omega,f_0)}{f_0}$$

$$T_{f2}(\omega) := \frac{u_{f2}(0,\omega,f_0)}{f_0} \qquad T_s(\omega) := \frac{u_s(l_s,\omega,f_0)}{f_0} \qquad T_{e2}(\omega) := \frac{u_{e2}(0,\omega,f_0)}{f_0}$$

For Spring-Mass Boundary Condition

$$f_m = u_s(l_s)\left(k - \frac{k^2}{k - m\omega^2}\right) \longrightarrow M1(\omega), M2(\omega)$$

Fig. 12 Solving 1-D model for longitudinal mode bolt resonances using matrices.

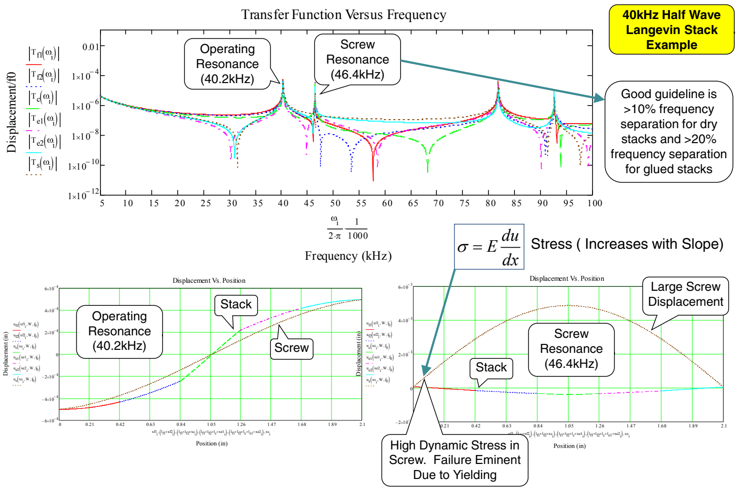

Fig. 13 Example of 1-D model results for longitudinal mode bolt resonance prediction.

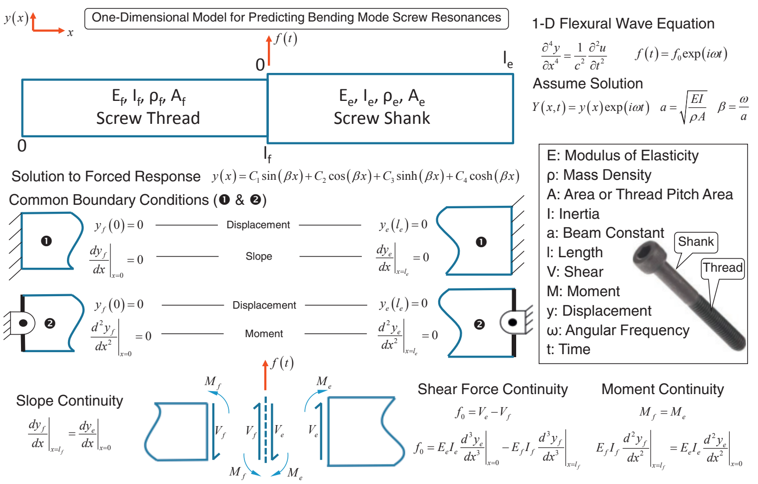

Fig. 14 1-D modeling for predicting bending mode bolt resonances.

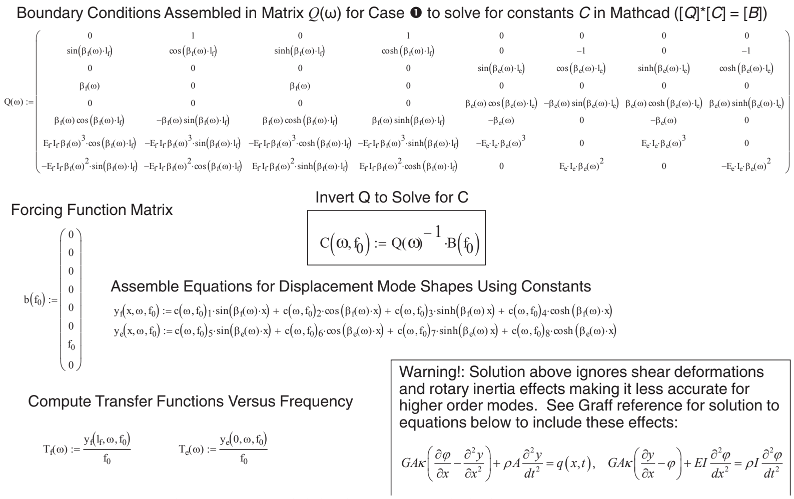

Boundary Conditions Assembled in Matrix $Q(\omega)$ for Case ❶ to solve for constants C in Mathcad ($[Q]*[C] = [B]$)

$$Q(\omega) := \begin{pmatrix} 0 & 1 & 0 & 1 & 0 & 0 & 0 & 0 \\ \sin(\beta_f(\omega)\cdot l_f) & \cos(\beta_f(\omega)\cdot l_f) & \sinh(\beta_f(\omega)\cdot l_f) & \cosh(\beta_f(\omega)\cdot l_f) & 0 & -1 & 0 & -1 \\ 0 & 0 & 0 & 0 & \sin(\beta_e(\omega)\cdot l_e) & \cos(\beta_e(\omega)\cdot l_e) & \sinh(\beta_e(\omega)\cdot l_e) & \cosh(\beta_e(\omega)\cdot l_e) \\ \beta_f(\omega) & 0 & \beta_f(\omega) & 0 & 0 & 0 & 0 & 0 \\ 0 & 0 & 0 & 0 & \beta_e(\omega)\cos(\beta_e(\omega)\cdot l_e) & -\beta_e(\omega)\sin(\beta_e(\omega)\cdot l_e) & \beta_e(\omega)\cosh(\beta_e(\omega)\cdot l_e) & \beta_e(\omega)\sinh(\beta_e(\omega)\cdot l_e) \\ \beta_f(\omega)\cos(\beta_f(\omega)\cdot l_f) & -\beta_f(\omega)\sin(\beta_f(\omega)\cdot l_f) & \beta_f(\omega)\cosh(\beta_f(\omega)\cdot l_f) & \beta_f(\omega)\sinh(\beta_f(\omega)\cdot l_f) & -\beta_e(\omega) & 0 & -\beta_e(\omega) & 0 \\ E_f\cdot I_f\cdot\beta_f(\omega)^3\cdot\cos(\beta_f(\omega)\cdot l_f) & -E_f\cdot I_f\cdot\beta_f(\omega)^3\cdot\sin(\beta_f(\omega)\cdot l_f) & -E_f\cdot I_f\cdot\beta_f(\omega)^3\cdot\cosh(\beta_f(\omega)\cdot l_f) & -E_f\cdot I_f\cdot\beta_f(\omega)^3\cdot\sinh(\beta_f(\omega)\cdot l_f) & -E_e\cdot I_e\cdot\beta_e(\omega)^3 & 0 & E_e\cdot I_e\cdot\beta_e(\omega)^3 & 0 \\ -E_f\cdot I_f\cdot\beta_f(\omega)^2\cdot\sin(\beta_f(\omega)\cdot l_f) & -E_f\cdot I_f\cdot\beta_f(\omega)^2\cdot\cos(\beta_f(\omega)\cdot l_f) & E_f\cdot I_f\cdot\beta_f(\omega)^2\cdot\sinh(\beta_f(\omega)\cdot l_f) & E_f\cdot I_f\cdot\beta_f(\omega)^2\cdot\cosh(\beta_f(\omega)\cdot l_f) & 0 & E_e\cdot I_e\cdot\beta_e(\omega)^2 & 0 & -E_e\cdot I_e\cdot\beta_e(\omega)^2 \end{pmatrix}$$

Forcing Function Matrix

$$b(f_0) := \begin{pmatrix} 0 \\ 0 \\ 0 \\ 0 \\ 0 \\ 0 \\ f_0 \\ 0 \end{pmatrix}$$

Invert Q to Solve for C

$$\boxed{C(\omega, f_0) := Q(\omega)^{-1}\cdot B(f_0)}$$

Assemble Equations for Displacement Mode Shapes Using Constants

$$y_f(x,\omega,f_0) := c(\omega,f_0)_1\cdot\sin(\beta_f(\omega)\cdot x) + c(\omega,f_0)_2\cdot\cos(\beta_f(\omega)\cdot x) + c(\omega,f_0)_3\cdot\sinh(\beta_f(\omega)\,x) + c(\omega,f_0)_4\cdot\cosh(\beta_f(\omega)\cdot x)$$

$$y_e(x,\omega,f_0) := c(\omega,f_0)_5\cdot\sin(\beta_e(\omega)\cdot x) + c(\omega,f_0)_6\cdot\cos(\beta_e(\omega)\cdot x) + c(\omega,f_0)_7\cdot\sinh(\beta_e(\omega)\,x) + c(\omega,f_0)_8\cdot\cosh(\beta_e(\omega)\cdot x)$$

Compute Transfer Functions Versus Frequency

$$T_f(\omega) := \frac{y_f(l_f,\omega,f_0)}{f_0} \qquad T_e(\omega) := \frac{y_e(0,\omega,f_0)}{f_0}$$

Warning!: Solution above ignores shear deformations and rotary inertia effects making it less accurate for higher order modes. See Graff reference for solution to equations below to include these effects:

$$GA\kappa\left(\frac{\partial\varphi}{\partial x} - \frac{\partial^2 y}{\partial x^2}\right) + \rho A\frac{\partial^2 y}{dt^2} = q(x,t), \quad GA\kappa\left(\frac{\partial y}{\partial x} - \varphi\right) + EI\frac{\partial^2\varphi}{dx^2} = \rho I\frac{\partial^2\varphi}{dt^2}$$

Fig. 15 Solving 1-D model for bending mode bolt resonances using matrices.

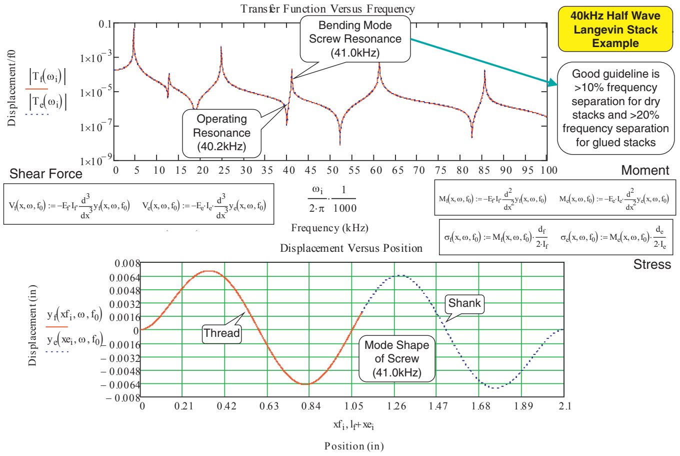

Fig. 16 Example of 1-D model results for bending mode bolt resonance prediction.

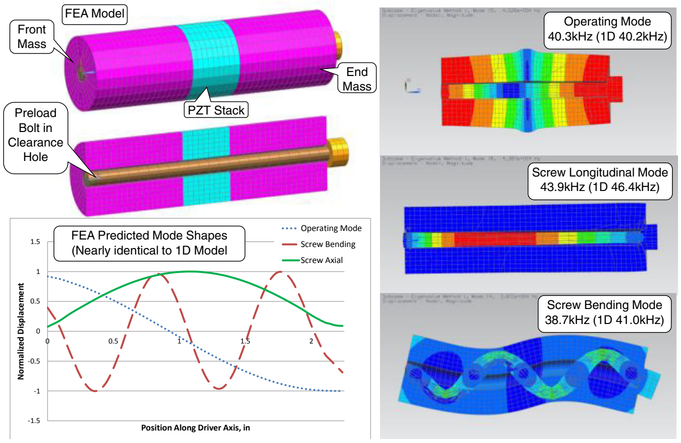

Fig. 17 Comparison of 1-D model of the 40kHz half wave Langevin stack solution to FEA model.

7. Conclusions

The preload screw configuration and design requires a detailed trade-off analysis to optimize stress uniformity, e-mech coupling and stack symmetry, while minimizing interaction of parasitic screw modes. Screw resonances can manifest as both longitudinal and bending modes. Actual boundary conditions can be tricky to model in FEA making prediction difficult. Commonly used axisymmetric FEA models cannot predict screw bending modes. Screw boundary conditions can especially vary with glued piezo stack designs, so greater separation with parasitic screw modes is required compared to dry stacks. Uncontrolled screw resonances often lead to preload loss and screw failure, but at the very least they can negatively affect transducer performance. The best bolt material is the one with the highest yield strength σ_y and the lowest stiffness or elastic modulus E, i.e., maximize the ratio σ_y /E. The phase window or coupling k is maximized when the bolt stiffness is minimized relative to piezo stack. The sizing of preload screws and determination of minimum thread engagement should always be done based on yield strength (yielding = preload loss). An adequate thread engagement length based on yield stress is critical for both the preload screw and internal threads of horn to prevent preload loss under dynamics. Uniformity of prestress effects both bolt sizing and e-mech coupling. Simple 1-D wave equation models can be a fast and effective way to identify locations of parasitic screw resonance for many piezo stack configurations. For parasitic bolt resonances, use 10% frequency separation for dry stacks and 20% frequency separation for glued stacks.

References

C. H. Sherman and J. L. Butler, Transducers and Arrays for Underwater Sound. New York, NY: Springer Science, 2007.
D. A. DeAngelis and D. C. Schalcosky, "The Effect of PZT8 Piezoelectric Crystal Aging on Mechanical and Electrical Resonances in Ultrasonic Transducers," 2006 IEEE Ultrasonics Symposium, Session P2O-10.
D. A. DeAngelis and G. W. Schulze, "Advanced Bode Plot Techniques for Ultrasonic Transducers," 2011 UIA Symposium Proceedings, Physics Procedia.
D. A. DeAngelis and G. W. Schulze, "Optimizing Piezoelectric Ceramic Thickness in Ultrasonic Transducers," 2010 UIA Symposium Proceedings, IEEE XPlore.
D. A. DeAngelis and G. W. Schulze, "Optimizing Piezoelectric Crystal Preload in Ultrasonic Transducers," 2009 UIA Symposium Proceedings, IEEE XPlore.
D. A. DeAngelis and G. W. Schulze, "The Effects of Piezoelectric Ceramic Dissipation Factor on the Performance of Ultrasonic Transducers," 2012 UIA Symposium Proceedings, Physics Procedia.
D. Stansfield, Underwater Electroacoustic Transducers. Los Altos, CA: Peninsula Publishing, 1991.
K. F. Graff, Wave Motion in Elastic Solids. New York, NY: Dover Publications, 1991.
K. Uchino and J. R. Giniewicz, Micromechatronics. New York, NY: Marcel Dekker, 2003.
K. Uchino, Ferroelectric Devices. New York, NY: Marcel Dekker, 2010.
O. B. Wilson, Introduction to Theory and Design of Sonar Transducers. Los Altos, CA: Peninsula Publishing, 1991.
R. A. Walsh, Electromechanical Design Handbook. Blue Ridge Summit, PA: TAB Books, 1990.
R. S. Woollett, "Transducer Comparison Methods Based on the Electromechanical Coupling-Coefficient Concept," 1957 IRE National Convention, p. 23-27, IEEE Xplore.